CHEMISTRY & BIODIVERSITY

Accepted Article

Title: Water-Soluble Curcumin Derivatives Including Aza-Crown Ether Macrocycles as Enhancers of their Cytotoxic Activity.

Authors: David Morales-Morales, Antonino Arenaza-Corona, Paola Sánchez-Portillo, Lucero González-Sebastián, Arturo Sánchez-Mora, Brian Monroy-Torres, Teresa Ramírez-Apan, Nicolás Puentes-Díaz, Jorge Alí-Torres, Victor Barba, and Viviana Reyes-Marquez

To be cited as: *Chem. Biodiversity* **2024**, e202402083

Link to VoR: https://doi.org/10.1002/cbdv.202402083

www.cb.wiley.com

WILEY-VHCA

10.1002/cbdv.202402083

Water-Soluble Curcumin Derivatives Including Aza-Crown Ether Macrocycles as Enhancers of their Cytotoxic Activity.

Antonino Arenaza-Corona,[a,*] Paola Sánchez-Portillo,[d] Lucero González-Sebastián[b], Arturo Sánchez-Mora,[a] Brian Monroy-Torres,[a] Teresa Ramírez-Apan,[a] Nicolás Puentes-Díaz,[c] Jorge Alí-Torres,[c] Victor Barba,[d] Viviana Reyes-Marquez[e] and David Morales Morales[a,*]

[a]*Instituto de Química, Universidad Nacional Autónoma de México, Circuito Exterior, Ciudad Universitaria, Mexico City C.P. 04510 (Mexico).* [b]*Universidad Autónoma Metropolitana-Iztapalapa, Av. San Rafael Atlixco No. 186, Ciudad de México, C.P. 09340, México.* [c]*Departamento de Química, Universidad Nacional de Colombia- Sede Bogotá Bogotá 111321 (Colombia).* [d]*Centro de Investigaciones Químicas-IICBA, Universidad Autónoma del Estado de Morelos. Av. Universidad 1001, Col. Chamilpa, Cuernavaca, Morelos C. P. 62209 (Mexico).* [e]*Departamento de Ciencias Químico-Biológicas, Universidad de Sonora, Luis Encinas y Rosales s/n, Hermosillo C.P. 83000, Sonora, Mexico.*

E-mail: damor@unam.mx

Graphical Abstract

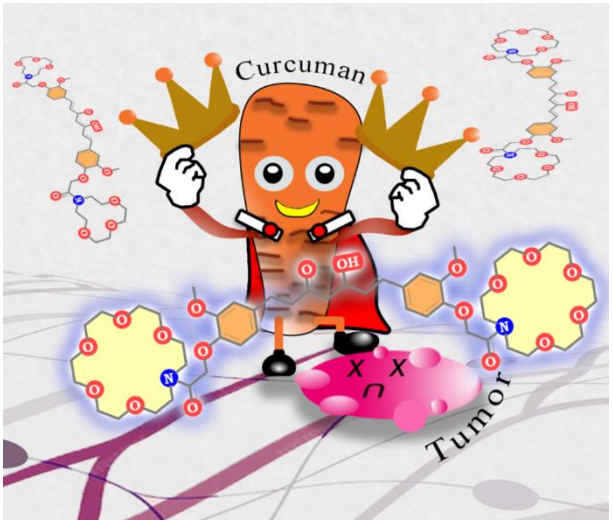

Abstract

The synthesis of three novel curcumin derivative compounds, featuring aza-crown ether macrocycles of various sizes (aza-12-crown-4, aza-15-crown-5, and aza-18-crown-6), is described. The incorporation of these aza-crown macrocycles significantly enhances their water solubility, positioning them as groundbreaking instances of curcumin derivatives that are fully soluble in aqueous environments. These curcumin ligands (**L1**, **L2**, and **L3**) were

10.1002/cbdv.202402083

then reacted with zinc acetate to afford the coordination metal complexes (**L1-Zn**, **L2-Zn**, and **L3-Zn**). Comprehensive characterization of all compounds was achieved using various analytical techniques, including 1D and 2D NMR spectroscopy, ATR-FTIR spectroscopy, mass spectrometry (ESI^+), elemental analysis and UV-Vis spectroscopy. The *in vitro* cytotoxic activity of both, ligands and complexes were evaluated on three human cancer cell lines (U-251, MCF-7, and SK-LU-1). Compared to conventional curcumin, these compounds demonstrated improved antiproliferative potential. Additionally, a wound healing assay was conducted to assess their antimigration properties. The obtained results suggest that these modifications to the curcumin structure represent a promising approach for developing therapeutic agents with enhanced cytotoxic properties.

Keywords: Curcumin Zinc Complexes; Water-Soluble Curcumin Derivatives; Crown Ether Metallodrugs; Antiproliferative Activity; Molecular Docking.

1. Introduction

In the ongoing pursuit of effective therapies for proliferative diseases, there has been a remarkable surge in interest surrounding natural bioactive compounds. Notably, curcumin, extracted from the rhizomes of *Curcuma longa*, has emerged as a promising candidate due to its multifaceted potential in therapeutic intervention. This polyphenol exhibits a wide array of activities, including anti-inflammatory,[1] antioxidant,[2,3] antitumoral,[4–7] antimicrobial, antiviral, chemotherapeutic[8] effects, and serves as a wound healing agent.[9,10] However, despite these beneficial attributes, its application in medicine is constrained by challenges such as low stability, limited bioavailability and rapid metabolism.[11]

As a result, the design of curcumin-based compounds by incorporating various groups into its framework has become a key area of interest in current research. For instance, efforts to enhance its transport and bioavailability have led to the incorporation of cyclodextrins, resulting in curcumin derivative compounds soluble in water and with increased dispersibility. Additionally, other strategies[12] include attaching curcumin to dendrimer supports and organic polymers[13] as well as developing co-drugs such as piperine,[14–16] all aimed at improving its bioavailability.

Given the fact that the β-diketone system within the curcumin structure serves as a chelate for metal complex formation, this trait has been harnessed to produce a range of curcumin-metal compounds incorporating diverse divalent and trivalent metals. This approach enhances the stability and bioavailability of curcumin derivatives, thereby amplifying their biological activity.[17–19] In this context, the zinc metal center, has been shown to enhance the activity of these curcuminoids.[20] Another successful strategy employed involves structural modifications of the parent molecule, including substitutions on the OH group of the phenol with either aliphatic or acetyl chains.[21,22]

Thus, the structural modification of curcumin has rendered valuable derivatives as therapeutic agents, achieved by incorporating specific molecules that enhance the stability, transportation, and bioavailability of its derivatives. In this context, aza-crown ethers that are supramolecular macrocycles possessing an amphiphilic nature[23] and noted for their antitumor activity,[24] have been selected to be incorporated in the curcumin periphery. The aim is to develop molecules soluble in physiological environments, potentially boosting their biological activity and offering new avenues for advancing antitumor treatments. Hence, in

this study, we detail the synthesis of three novel curcumin derivatives, which incorporate aza-crown ether macrocycles of various sizes (aza-12-crown-4, aza-15-crown-5, and aza-18-crown-6), along with their zinc complexes. Additionally, we investigated their *in vitro* cytotoxic activity on six human cancer cell lines and conducted a wound healing assay. Our hypothesis posits that the incorporation of aza-crown ethers into the curcumin structure could enhance physiological solubility, cytotoxicity, stability, and bioavailability.

2. Results and Discussion

2.1 Synthesis and characterization

The synthesis of **L1**-**L3** is outlined in Scheme 1. Precursors A-C, comprising crown ethers of various sizes in the form of 2-chloroacetylamides, were synthesized using a modified procedure previously reported. These precursors were fully characterized by NMR and mass spectroscopy and structurally confirmed through direct comparison with previously reported data (detailed information is provided in the experimental section).[25] Subsequently, the 2-chloroacetylamide derivatives were reacted with curcumin in the presence of KI as the halogen exchanger and Cs_2CO_3 as a base, yielding compounds **L1**-**L3** as semisolids at room temperature. It was observed that the melting points of **L1**-**L3** decreased with increasing size of the macrocycle.

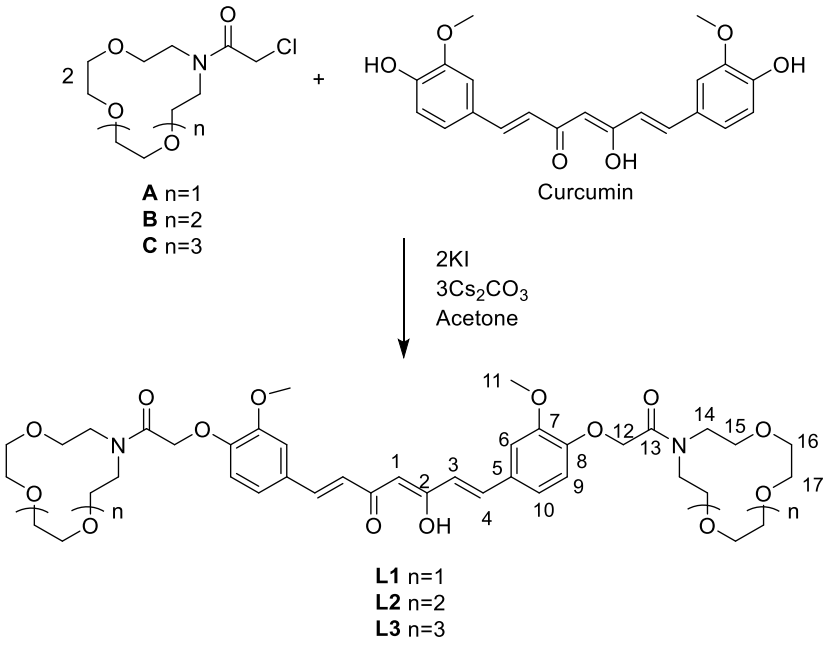

Scheme 1. General synthesis of curcuminoids bearing aza-crown ethers.

The three ligands were characterized using ATR-FTIR spectroscopy. The absence of the band at ν = 1499 cm^{-1}, assigned to the -OH (phenol group) from the starting curcumin, along with the observed band around ν = 1581 cm^{-1} in **L1**-**L2**, assigned to the carbonyl from the amide group, confirms the substitution of the alcohol proton by the aza-crown ethers. Additionally, the frequencies of the carbonyl groups from enol and vinyl fragments (C=O and C=C) are observed to be slightly shifted to lower energy vibrations, approximately 20 cm^{-1} lower than those of curcumin (ν = 1626 and ν = 1601 cm^{-1}, respectively) (see Figures S11, S12, S13). The proposed structures of **L1**-**L2** were also further confirmed by ^{1}H NMR, where characteristic signals from the curcumin fragment and proton resonances from the ether crown were observed in the NMR spectra. Specifically, the proton signal from the methylene amide group appeared around δ = 4.8 ppm in all ligands. In the ^{13}C NMR spectra, the signal of carbonyl of the amide group was observed around δ = 168 ppm, while the methylene groups of ether crown were localized in the range of δ = 50-70 ppm (see Figures S20, S21 and S22). Additional evidence for the formation of compounds **L1**-**L3** was obtained from mass spectrometric analysis. The ESI^{+} mass spectra displayed peaks corresponding to the mass cluster with sodium cation at m/z = 821.3, 908.9, and 996.9 for **L1**, **L2**, and **L3**, respectively (refer to Figures S14, S15, and S16 in the supporting information). Elemental analysis studies corroborate the percentages of the elements present in the molecules **L1**-**L3**, despite the nature of crown ethers, which tend to absorb humidity from the environment.

With the ligands in hand and considering that the incorporation of metals into the curcuminoid backbone could enhance their antitumor activity, as a proof-of-concept, the ligands **L1**-**L3** were metalated through a simple reaction with zinc acetate (see Scheme 2) to yield the coordination metal complexes **L1**-**Zn** to **L3**-**Zn**.

The Zn(II) complexes were characterized in solution by ^{1}H NMR, revealing a shift in the resonance of the methine protons to lower frequencies compared to those of the free ligands **L2**-**L3** (from δ = 6.1 to 5.7 ppm) due to the coordination to the metal center through the keto-enol chelate moiety. Additionally, zinc coordination was also inferred by ATR-FTIR, where the displacement of the stretching band of the central carbonyl group was shifted to lower frequencies than those observed in the free ligands ($\Delta\nu$ =10-15 cm^{-1}) (see spectra in the SI). Furthermore, the mass spectrometry analysis by MALDI-TOF allowed the detection of a

10.1002/cbdv.202402083

water adduct for complex **L1-Zn**, the molecular ion of **L2-Zn**, while the expected fragmentation pattern for complex **L3-Zn** was observed, moreover, results obtained from elemental analysis also are consistent with the chemical composition of the hydrated zinc complexes (see Figures S23-S34).

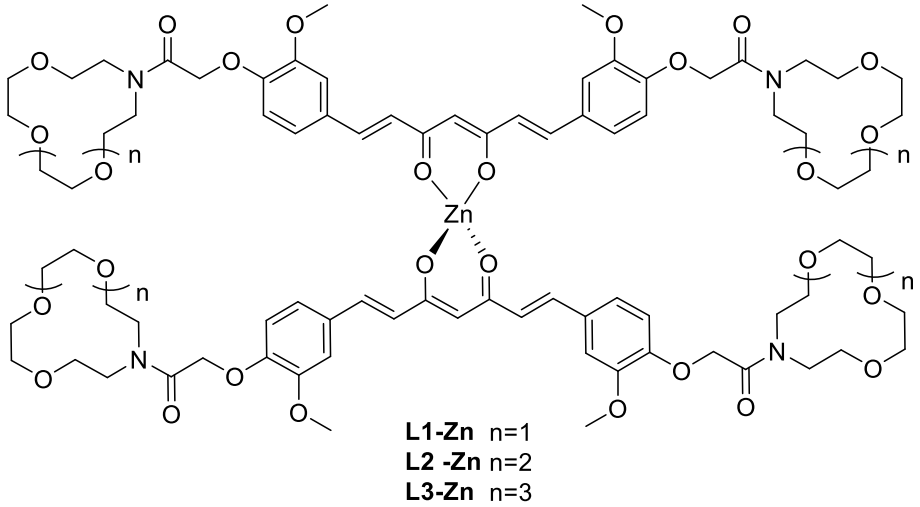

Scheme 2. Coordination of Zinc in curcuminoid derivatives bearing aza-crown ethers.

2.2 Antitumoral activity

The *in vitro* cytotoxic activity of all ligands and complexes was assessed against six cancer cell lines: glioblastoma (U-251), prostatic adenocarcinoma (PC-3), chronic myelogenous leukemia lymphoma (K-562), colorectal adenocarcinoma (HCT-15), mammary adenocarcinoma (MCF-7), and lung adenocarcinoma (SKLU-1), along with a non-cancerous green monkey kidney (COS-7) cell line for comparative purposes. The study also included evaluation of the curcumin molecule and cisplatin. Initially, the cytotoxic activity was investigated using a concentration of 25 µM. However, all compounds were found to be highly active on all cell lines, showing total inhibition (Table 1). Therefore, the concentration was reduced to 5 µM, and the results are shown in Table 1.

Table 1. Cytotoxic activity of ligands and complexes at 5 µM.

		% growth inhibition by cell line					
Comp.	**U251**	**PC-3**	**K562**	**HCT-15**	**MCF-7**	**SKLU-1**	**COS7**
L1	11.68	11.43	NC	25.01	NC	6.27	8.58
L2	21.42	11.43	22.40	18.09	4.69	20.8	12.27
L3	13.82	4.14	34.10	15.74	39.01	39.34	34.70
L1-Zn	NC	NC	41.22	NC	38.02	29.2	22.20
L2-Zn	NC	NC	72.77	NC	46.09	46.31	31.30
L3-Zn	78.82	10.61	34.61	66.59	70.0	75.19	39.11

NC = No cytotoxicity was observed.

In general, the zinc coordination complexes demonstrated superior cytotoxic activity compared to the ligands **L1**-**L3** against three cancer cell lines: U-251, MCF-7, and SKLU-1, as well as the healthy cell line COS-7. Notably, the highest cytotoxic activity was observed with **L3** and **L3-Zn**. Given the significant growth inhibition observed across U-251, MCF-7, and SKLU-1 cell lines, their IC_{50} parameters were determined (see Table 2). Notably, as shown in Table 2, all ligand compounds and their zinc complexes demonstrated significantly higher cytotoxic activity compared to the pharmaceutical ingredient curcumin. For instance, in U-251, the activity increased 3 to 5-fold, as depicted in Figure 1. Particularly, the complex **L3-Zn** exhibited the best antitumoral activity against U-251 (4.0±0.1), MCF-7 (4.0±0.6), and SKLU-1 (3.7±0.3). These values are similar to those found for cisplatin (Table 2). The high activity exhibited by complex **L3-Zn** could be attributed to the enhancement in cellular uptake facilitated by the amphiphilic moiety, which is influenced by the size of the crown ether.

Table 2. IC_{50} values obtained for ligands **L1**-**L3**, **Zn**-complexes, curcumin and cisplatin in µM against human cancer cell lines.

Comp.	**U-251**	**MCF-7**	**SK-LU-1**
Curcumin	20.5±1.7	18.4±0.9	12.9±0.7

L1	6.8±0.1	10.8±0.3	12.7±0.8
L2	5.9±0.4	8.4±0.4	9.3±0.8
L3	5.4±0.3	4.8±0.8	6.2±0.2
L1-Zn	5.0±0.4	6.4±0.7	6.3±0.7
L2-Zn	4.4±0.4	5.1±0.3	3.6±0.2
L3-Zn	4.0±0.1	4.0±0.6	3.7±0.3
Cisplatin	4.7±0.2	9.4±0.3	4.3±0.3

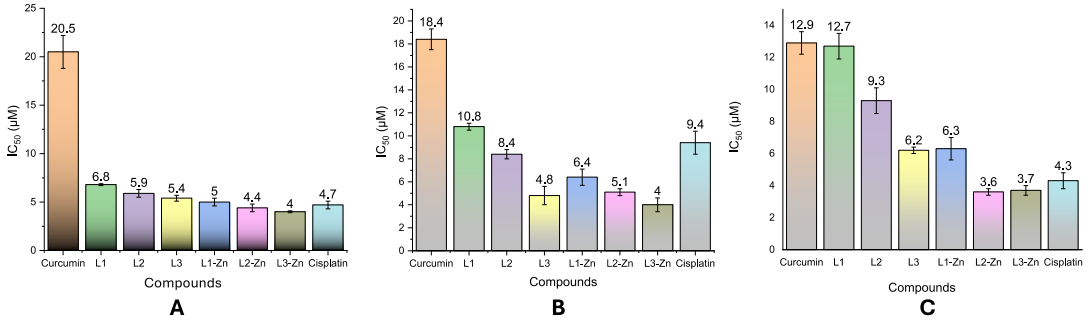

Figure 1. Graphics of IC_{50} (μM) of the compounds against cell lines: A) U-251, B) MCF-7 and C) SKLU-1.

2.3 Wound Healing Assay

As is known, cell migration in human cells is a physiological characteristic, but it is also related to a hallmark in cancer progression, particularly in invasion and metastasis.[26] Because of that the wound healing potential of curcuminoid compounds were investigated in two cell lines (SK-LU-1 and U-251). In the Figure 2 can be detected that the untreated control cancer cells migrate in a time-dependent manner due to the metastatic properties of the cell line. In general, when the cell lines were treated with **L1**, **L2**, and **L3** and their zinc analogues, a better performance of the zinc complexes was observed, except for the comparative activity of **L3** and **L3-Zn**. In the SK-LU-1 cell line, the zinc complex **L1-Zn** achieved the best

10.1002/cbdv.202402083

activity, decreasing cell migration by almost 30%. Meanwhile, in the U-251 cell line, the greatest decrease was observed with **L2-Zn**. These results strongly suggest that the Zn atom plays a central role in the cell migration behavior of the curcuminoid complexes.

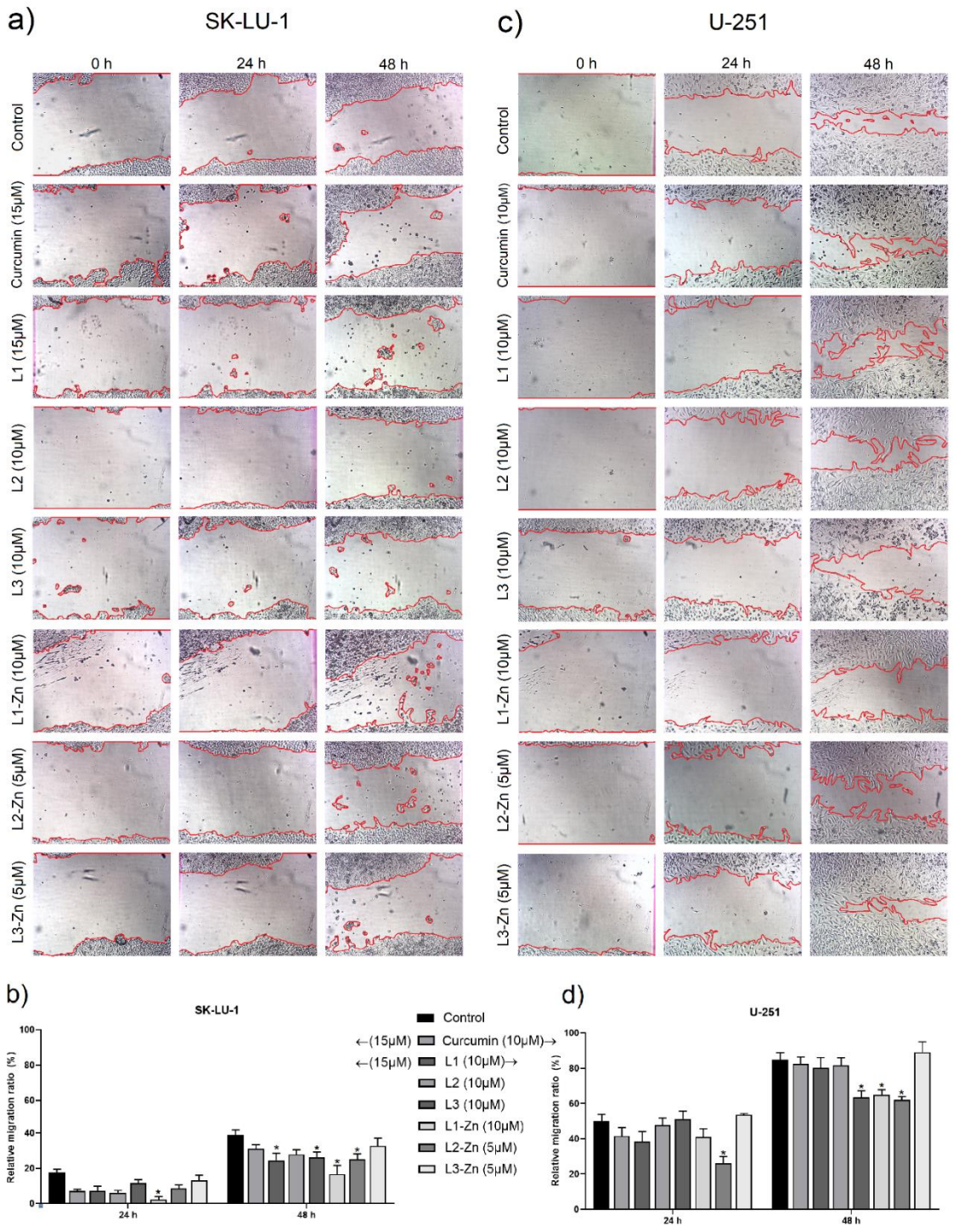

Figure 2. Curcuminoids effect in cell migration of SK-LU-1 (a-b) and U-251 (c-d) cell lines by the Wound Healing Assay. Microscopies were captured at 24 and 48 h, and the relative ratio was calculated. Data expressed as mean ± SEM and ** $p < 0.05$ (2way ANOVA).

2.4 Molecular docking simulations

The binding modes of compounds **L3** and **L3-Zn** with the target proteins for the K-562, MCF-7 and SK-LU-1 cell lines were predicted, and the values obtained for the scoring function are shown in Table 3. All obtained values ranged between -8.2 and -13.0 kcal/mol, with no drastic differences in affinity scores. However, higher values were achieved for the **L3-Zn** complexes in all three cell lines due to the larger size of the complexes and their flexible structures, which allowed them to adapt to the targets surfaces and enhance hydrophobic interactions.

Table 3. Score function values were obtained for compounds **L3** and **L3-Zn,** and the target proteins related to K-562 and MCF-7 cell lines.

Target	L3	L3-Zn	Target	L3	L3-Zn
K-562					
5VKM	-9.3	-10.1	2W96	-10.0	-11.6
5XY1	-10.9	-10.2	3G33	-9.7	-11.2
6HM6	-9.8	-9.8	3NUP	-9.2	-11.6
6HRP	-11.3	-12.0	1QPJ	-11.3	-11.5
3CS9	-11.7 [a]	-10.3	1XZ0	-9.6	-13.2 [a]
1FIN	-10.6	-12.1	2DQ7	-11.1	-12.6
1W98	-9.8	-11.0	4XJS	-9.7	-11.2
MCF-7					
2J6M	-9.9	-10.8	4OAR	-9.6	-11.9 [a]
3HY3	-9.4	-9.9	6CHZ	-10.3	-11.8
4FA2	-11.1 [a]	-11.7			
SK-LU-1					
1M17	-10.1	-12.0	3ZBF	-9.4	-11.6

10.1002/cbdv.202402083

3DKC	-10.1	-11.1	4CKJ	-10.7 [a]	-13.0 [a]
3LMG	-8.9	-9.9	5FTO	-10.1	-11.2

[a] Best score values per cell line for each compound.

Our results suggest that the best affinities are to be expected for the following cell lines targets: K562, ABL kinase (3CS9) and the cluster of differentiation **L3-Zn** (1XZ0); MCF-7, the mitogen-activated kinase (4FA2) and the progesterone receptor (4OAR); and SK-LU-1, RET tyrosine kinase (4CKJ). The best-interacting poses for the latter interactions are depicted in Figure 3. As shown, the coordination modes exhibit several hydrophobic interactions, with H-bondings present in some cases; the latter being established through polar interactions with the available oxygen atoms present in the ether, central keto/hydroxy, and amide groups of the ligands. These modes show that both compounds can adapt to the protein target active site and/or near surface. These score values and their best binding modes suggest that compounds **L3** and **L3-Zn** can inhibit the target's biological activity in cancer cells potentially disrupting their proliferation.

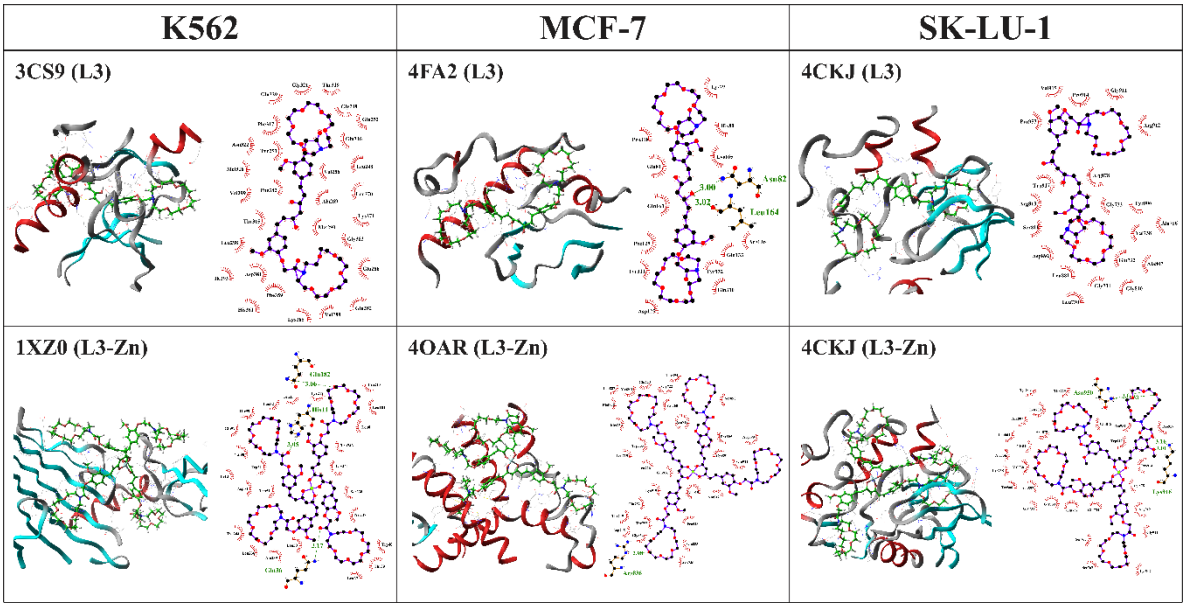

Figure 3. Suggested interaction of compounds **L3** and **L3-Zn** with their best-performing target protein of each cell line. The 3D representation shows the secondary structure of the target in red (alpha helix) and cyan (beta sheets), and the compounds in green balls & sticks display. The 2D representations show compound atoms colored in black (C), red (O), blue (N), and green (Zn).

2.5 Partition coefficient

The water insolubility of curcumin was overcome by its functionalization with crown ethers, which enhanced its bioavailability and, consequently, increased its cytotoxicity. In this study, the partition coefficient analysis was also considered to demonstrate the water solubility of the compounds and assess their distribution capacity in both lipid and aqueous media. This analysis is crucial in the drug development phase as it helps to evaluate the capacity of the drug to effectively traverse biological barriers, dissolve in lipid-rich tissues or aqueous media, and achieve efficient absorption within an organism. The partition coefficient (Log D) was determined using a physiological phosphate buffer at pH 7.4 in *n*-octanol by the shake-flask method and analyzed via HPLC.[27] According to the results, the compounds are more hydrophilic when the oxygens in the crown moiety increase. On the other hand, when the Log D value of **L1-L3** and their zinc complexes was compared, an insignificant difference was observed between them (Table 4). The Log *D* values obtained for all analysed compounds ranged between 2.6 and 3.2, indicating that the ligands and zinc complexes possess favourable lipophilicity for potential drug development. This strikes a balance between water solubility and membrane permeability, which is essential for their bioavailability and therapeutic efficacy.

Table 4. Partition coefficient (log D o/w) of potent compounds.

Compound	L1	L2	L3	L1-Zn	L2-Zn	L3-Zn
Log*D*	3.2	2.8	2.7	3.2	2.7	2.6

2.6 UV-Vis studies

All ligands **L1-L3** were analysed by UV-Vis spectroscopy using methanol and water as solvents. A comparative UV-Vis spectra of the ligands and curcumin is shown in Figure 4 (see also S32), while the absorption maxima and molar absorptivity coefficients are summarized in Table 5. The **L1-L3** compounds showed maximum absorptions in methanol in the range of λ_{max} = 330 - 370 nm owing to the π-π* transitions,[28,29] and these increase with the size of the crown ether substituent, while the molar absorption coefficient decrease.

10.1002/cbdv.202402083

Furthermore, a hypsochromic shift of the ligands compared with the value for curcumin (425 nm) was observed. The presence of more than one shoulder in **L1** spectra indicates the possible presence of more than one isomeric form in the ground state.[30,31] When the solvent polarity was increased by using water, the opposite trend was observed; the values of maximum absorptions increased with the macrocycle size, which agrees with the partition coefficient.

Table 5. Absorption maxima (λ max) and molar absorptivity coefficient (ε) of compounds **L1**, **L2**, **L3** and curcumin in methanol and water.

	λ_{max} (nm) / ε ($Lmol^{-1}cm^{-1}$)	
Compound	**Methanol**	**Water**
L1	330/13483	325/6384
L2	365/11738	360/11212
L3	370/8955	360/14895
Curcumin	425/23734	ND

ND. Not determinate.

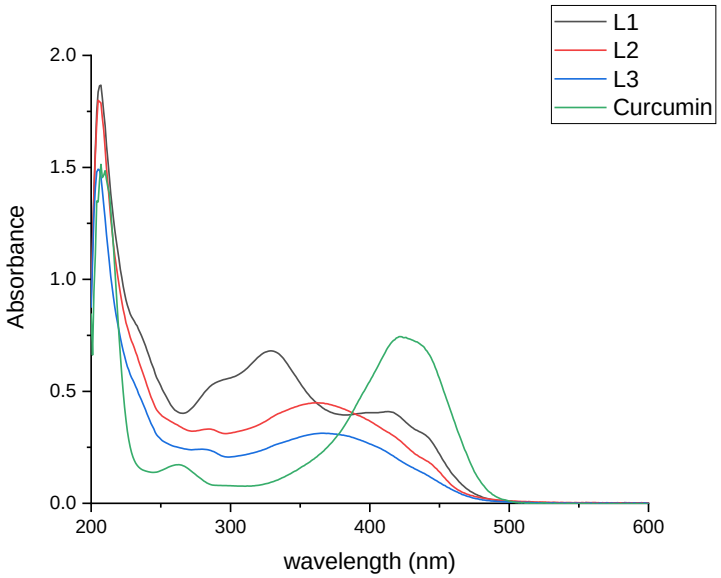

Figure 4. Overlapped UV-Vis spectra of compounds **L1-L3** in methanol at $5x10^{-5}$ Molar concentration.

10.1002/cbdv.202402083

On the other hand, the sensing properties against monovalent and divalent metals were also investigated to observe the response to different cations. The behavior of the three ligands with different monovalent and divalent metal cations was found to be very similar (see Figures S36, and S37). However, slight changes upon the addition of iron and copper were observed, with bands appearing at 445 nm and 490 nm, respectively. Additionally, when the compound **L1** was treated with manganese, an increase in the band at 490 nm was detected (Figure 5). These results suggest that these compounds could be used as sensors for manganese, iron, and copper detection.

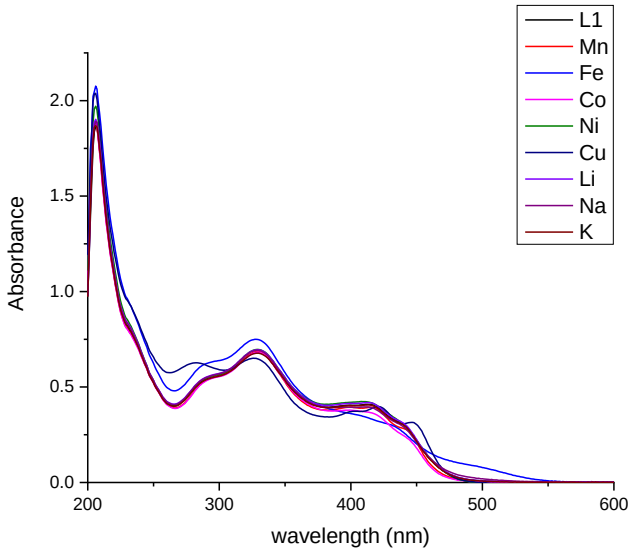

Figure 5. UV-Vis titration of the **L1** ligand with different cations.

3. Conclusion

Three new curcuminoids substituted with aza-crown ethers and their zinc complexes were synthesized and characterized using common analytical techniques. All compounds were found to be soluble in water. The antitumoral activity of all curcumin derivatives, including the parent curcumin, was tested against six cancer cell lines. It was found that **L3** and **L3-Zn** were active against three cell lines: U-251, MCF-7, and SKLU-1. Molecular docking simulations showed that **L3** and **L3-Zn** have similar binding score values towards a series of protein targets for each cancer cell line considered. Their best scoring coordination modes

exhibit multiple interactions, including hydrophobic and hydrogen bonds in some cases, and demonstrate good adaptation to the active sites and/or surrounding surface of the targets due to their flexibility and size, suggesting a capability to disrupt cancer cell proliferation.

Furthermore, UV-Vis studies revealed that π-π* transitions occur in the ligands L1-L3. From this analysis, it was detected that these ligands could offer a new alternative for cation sensing, specifically for manganese, iron, and copper.

This investigation opens new avenues for potential therapeutic applications of water-soluble curcumin derivatives in the treatment of proliferative disorders, especially in the context of their selective targeting toward U251, MCF7, and SKLU cell lines. The amplified antiproliferative potential exhibited by these derivatives offers promising prospects for targeted and effective interventions, bringing us closer to combating uncontrolled cell proliferation and improving patient outcomes.

4. Experimental

Aza-crowns (aza-12-crown-4, aza-15-crown-5, and aza-18-crown-6) and 2-chloroacetyl chloride were commercially available and purchased from Sigma-Aldrich. Pure curcumin was obtained from synthesis as previously reported.[32] All solvents were purified by conventional methods prior to use.

4.1 Synthesis of compounds

4.1.1 General synthesis of precursors **(A-C).**

0.2 g of the corresponding aza crown ether and 1.1 equivalents of sodium carbonate were dissolved in 40 mL of dichloromethane. Then, 1.5 equivalents of 2-chloroacetyl chloride were added, and the mixture was stirred overnight at -10 °C. Afterward, the solids were removed by filtration, and the solution was washed with 30 mL of 1 N HCl, followed by a wash with a solution of saturated Na_2CO_3. The organic phase was dried with sodium sulfate, resulting in the formation of a colourless oil.

4.1.2 General synthesis of ligands **L1-L3**.

Curcumin and 3 equivalents of cesium carbonate (Cs_2CO_3) were dissolved in 30 mL of acetone in a round-bottom flask. In another round-bottom flask, the precursors (A-C) with an

equimolar quantity of potassium iodide (KI) were dissolved in 20 mL of acetone and stirred for about 30 minutes. This suspension was then added dropwise to the first flask and refluxed overnight. Finally, the solids were removed by filtration, and the solution was evaporated. The residue was extracted at least three times with ethyl acetate and water (1:1). The organic phase was dried with sodium sulfate and evaporated under reduced pressure. The solid was dried under high vacuum.

L1 was obtained from 0.133 g (0.529 mmol) of precursor **A**, 0.098 g (0.265 mmol) of curcumin, 0.519 g of caesium carbonate (1.59 mmol), and 0.088 g of potassium iodide (0.53 mmol). Yield: 142 mg (67 %). MP = 80-83 °C. **ATR-FTIR** *v* = 1656 (C=O), 1623 (C=C), 1581 (C=O) cm^{-1}**.** **^{1}H NMR** (500 MHz, DMSO-d_6) δ = 7.57 (d, *J* = 15.8 Hz, 2H), 7.35 (d, *J* = 2.0 Hz, 2H), 7.18 (dd, *J* = 8.5, 2.0 Hz, 2H), 6.95 (d, *J* = 8.4 Hz, 2H), 6.80 (d, *J* = 15.9 Hz, 2H), 6.15 (s, 1H), 4.98 (s, 4H), 3.85 (d, *J* = 8.3 Hz, 6H), 3.68 – 3.64 (m, 4H), 3.58 (dq, *J* = 13.6, 4.8 Hz, 16H), 3.48 (dt, *J* = 12.3, 4.7 Hz, 8H), 3.42 (d, *J* = 4.6 Hz, 4H). **^{13}C NMR** (126 MHz, DMSO-d_6) δ = 183.2, 167.3, 150.0, 148.9, 140.4, 127.6, 122.7, 122.0, 112.8, 110.6, 100.8, 70.1, 69.5, 69.2, 69.0, 68.8, 67.9, 65.8, 55.7, 49.1, 48.8 ppm. **MS** (ESI^+) [$C_{41}H_{54}N_2O_{14}$] m/z, Actual mass = 798.36. Found mass = 821.3 $[M+Na]^+$. **Elemental Analysis:** [$C_{41}H_{54}N_2O_{14}$] Calculated: C, 61.64; H, 6.81; N, 3.51. Experimental: C, 61.28; H, 6.94; N, 3.27.

L2 was obtained from 0.276 g of precursor **B** (0.93 mmol), 0.172 g of curcumin (0.466 mmol), 0.455 g of caesium carbonate (1.4 mmol), and 0.155 g of potassium iodide (0.93 mmol). Yield: 304 mg (74 %). MP = 75-78 °C. **ATR-FTIR** *v* = 1657 (C=O), 1623 (C=C), 1582 (C=O) cm^{-1}. **^{1}H NMR** (500 MHz, DMSO-d_6) δ = 7.58 (d, *J* = 15.9 Hz, 2H), 7.36 (s, 2H), 7.20 (d, *J* = 8.3 Hz, 2H), 6.88 (d, *J* = 8.4 Hz, 2H), 6.82 (d, *J* = 15.9 Hz, 2H), 6.13 (s, 1H), 4.93 (s, 4H), 3.84 (s, 6H), 3.72 (t, *J* = 5.6 Hz, 8H), 3.55 (ddt, *J* = 23.2, 11.0, 5.6 Hz, 24H), 3.44 (t, *J* = 6.0 Hz, 8H). **^{13}C NMR** (126 MHz, DMSO-d_6) δ = 183.2, 167.3, 149.9, 149.0, 140.4, 127.8, 122.7, 122.1, 113.0, 110.8, 101.0, 70.4, 70.2, 69.6, 69.4, 69.4, 69.3, 68.1, 66.0, 55.7, 48.7, 48.3 ppm. **MS** (ESI^+) [$C_{45}H_{62}N_2O_{16}$] m/z, Actual mass = 886.41. Found mass = 908.9 $[M+Na]^+$. **Elemental Analysis:** [$C_{45}H_{62}N_2O_{16}$], Calculated: C, 60.94; H, 7.05; N, 3.16. Experimental: C, 59.74; H, 7.05; N, 3.29.

L3 was obtained from 0.115 g of precursor **C** (0.339 mmol), 0.0625 g of curcumin (0.169 mmol), 0.165 g of caesium carbonate (0.5 mmol), and 0.0562 g of potassium iodide (0.338 mmol). Yield: (132 mg) 40%. MP = 65-68 °C. **ATR-FTIR** *v* =1655 (C=O), 1624 (C=C), 1582 (C=O) cm^{-1}. **^{1}H NMR** (500 MHz, DMSO-d_6) δ = 7.57 (d, *J* = 15.8 Hz, 2H), 7.36 (d, *J* = 1.8 Hz, 2H), 7.22 (dd, *J* = 8.5, 1.8 Hz, 2H), 6.87 (d, *J* = 8.5 Hz, 2H), 6.83 (d, *J* = 15.9 Hz, 2H), 6.11 (s, 1H), 4.94 (s, 4H), 3.85 (s, 6H), 3.69 (t, *J* = 5.4 Hz, 8H), 3.63 – 3.46 (m, 40H). **^{13}C NMR** (126 MHz, DMSO-d_6) δ = 183.2, 167.2, 149.8, 149.0, 140.4, 127.8, 122.6, 122.1, 112.9, 110.9, 101.0, 70.3, 70.1, 70.0, 70.0, 69.9, 69.9, 69.8, 69.1, 68.3, 66.0, 55.7, 47.6, 46.1 ppm. **MS** (ESI^+) [$C_{49}H_{70}N_2O_{18}$] m/z, Actual mass = 974.46. Found mass = 996.9 $[M+Na]^+$. **Elemental Analysis:** [$C_{49}H_{70}N_2O_{18}$] Calculated: C, 60.36; H, 7.24; N, 2.87. Experimental: C, 59.41; H, 7.27; N, 2.95.

4.1.3 General synthesis of complexes **L-Zn**

The respective L1-L3 were dissolved in 20 mL of methanol, and 0.5 equivalents of anhydrous zinc acetate, previously dissolved in 10 mL of methanol, were added dropwise. The reaction was stirred for 24 hours. Afterward, the solvent was removed under reduced pressure, resulting in orange solids, which were then dried under high vacuum.

L1-Zn was obtained from 50 mg of **L1** (0.062 mmol) and 5 mg of zinc acetate anhydrous (0.031 mmol). Yield = 98%, MP = 116-119 °C. **ATR-FTIR** *v* = 1646 (C=O), 1622 (C=C), 1581 (C=O) cm^{-1}. **^{1}H NMR** (500 MHz, DMSO-d_6) δ = 7.4 (t, J = 14.9 Hz, 2H), 7.3 (d, J = 7.1 Hz, 2H), 7.1 (s, 2H), 6.9 (d, J = 8.3 Hz, 2H), 6.8 – 6.7 (m, 2H), 5.7 (s, 1H), 5.0 (s, 4H), 3.8 (s, 6H), 3.7 – 3.4 (m, 32H). **MS** (MALDI-TOF) [$C_{82}H_{116}N_4O_{25}Zn$] m/z, Actual mass = 1620.72. Found mass = 1620.510 $[M+H_2O]^+$. **Elemental Analysis:** [$C_{82}H_{106}N_4O_{28}Zn \cdot 5H_2O$], Calculated: C, 56.24; H, 6.68, N, 3.20. Experimental: C, 56.49; H, 6.41, N, 3.0.

L2-Zn was obtained from 34 mg of **L2** (0.038 mmol) and 3.5 mg of zinc acetate anhydrous (0.019 mmol). Yield = 99%. MP = 120-123 °C. **ATR-FTIR** *v* = 1643 (b, C=O and C=C), 1589 (C=O) cm^{-1}. **^{1}H NMR** (500 MHz, DMSO-d_6) δ 7.4 (d, J = 17.1 Hz, 2H), 7.3 (s, 2H), 7.1 (d, J = 7.9 Hz, 2H), 6.8 (d, J = 8.5 Hz, 2H), 6.7 (d, J = 15.6 Hz, 2H), 5.7 (s, 1H), 4.9 (s,

4H), 3.8 (s, 6H), 3.7 (t, J = 5.4 Hz, 8H), 3.6 – 3.4 (m, 24H). **MS** (MALDI-TOF) $[C_{90}H_{122}N_4O_{32}Zn]$ m/z, Actual mass = 1834.73. Found mass = 1836.84 $[M+2]^+$. **Elemental Analysis:** $[C_{90}H_{122}N_4O_{32}Zn \cdot 8H_2O]$, Calculated: C, 54.56; H, 7.02; N, 2.83. Experimental: C, 54.30, H, 6.54, N, 3.11.

L3-Zn was obtained from 30 mg of **L3** (0.03 mmol) and 3 mg of zinc acetate anhydrous (0.016 mmol). Yield = 98%. MP = 91-94 °C. **ATR-FTIR** *v* = 1641 (b, C=O and C=C), 1588 (C=O) cm^{-1}. **^{1}H NMR** (500 MHz, DMSO-d_6) δ = 7.6 (d, J = 15.7 Hz, 2H), 7.5 – 7.4 (m, 1H), 7.3 (s, 1H), 7.2 (d, J = 7.5 Hz, 1H), 7.1 (d, J = 7.4 Hz, 1H), 6.9 (d, J = 8.5 Hz, 2H), 6.7 (d, J = 15.7 Hz, 2H), 5.7 (s, 1H), 4.9 (d, J = 8.3 Hz, 4H), 3.8 (s, 6H), 3.8 – 3.4 (m, 48H). **MS** (MALDI-TOF) $[C_{98}H_{148}N_4O_{33}Zn]$ m/z, Actual mass = 1972.93. Found mass = 1971.581 $[C_{98}H_{148}N_4O_{33}Zn]^+$. **Elemental Analysis:** $[C_{98}H_{138}N_4O_{36}Zn \cdot 12H_2O]$, Calculated: C, 52.79, H, 7.32; N, 2.51. Experimental: C, 52.96, H, 6.52; N, 2.55.

4.2 Physical Measurements

Melting points were determined using an Electrothermal Engineering IA9100 × 1 melting point apparatus and are uncorrected.

4.3 Spectroscopic Determinations

The ATR-FTIR absorption spectra were recorded in the 4000–400 cm^{-1} range on a FT-IR NICOLET IS-50, Thermo Fisher Scientific spectrophotometer. Mass spectra were recorded in a Bruker Esquire 6000 with electrospray, atmospheric pressure chemical ionization and ion trap (ESI-TI, APCI-TI), Bruker Microflex with MALDI-Time of Flight (MALDI-TOF), and DART analysis was recorded in an AccuTOF JMS-T100LC equip. The ^{1}H, $^{13}C\{^1H\}$ NMR spectra were recorded on a Bruker 500 Ascend spectrometer, using DMSO-d_6 as solvent for the ligands and complexes. Elemental analyses were performed on a Thermo Scientific/Flash 2000 and a microbalance Mettler Toledo, XP6 model was used.

UV-Vis studies were performed using a Thermo Scientific Genesys 10S UV-Vis spectrophotometer in 3.5 mL quartz cells with a 1 cm path length, using methanol and water as solvents. All data treatments were analyzed with Origin software.[33] The molar absorption

coefficient was calculated using molar concentrations of $5x10^{-5}$, $4.6x10^{-5}$, 4.54 $x10^{-5}$, 4.35 $x10^{-5}$, 4.16 $x10^{-5}$, 4 $x10^{-5}$, 3.85 $x10^{-5}$ and 3.7 $x10^{-5}$. The cation metal sensing was carried out using equimolar solutions $5x10^{-5}$ M of curcumin derivatives (**L1**-**L3**) and cation metal ($MnCl_2$, $FeCl_2$, $CoCl_2$, $NiCl_2$, $CuCl_2$, $LiClO_4$, $NaClO_4$ and $KClO_4$).

4.4 Biological assays

The cytotoxicity activity of ligands **L1-L3** and complexes **L1-Zn**, **L2-Zn** and **L3-Zn** were tested against six cancer cell lines (purchased from Sigma-Aldrich): U-251 (human glioblastoma cell line), PC-3 (human Caucasian prostate adenocarcinoma), K562 (human Caucasian chronic myelogenous leukaemia), HCT-15 (human colon adenocarcinoma), MCF-7 (human mammary adenocarcinoma), and SK-LU-1 (human lung adenocarcinoma). The cell viability in the experiments exceeded 95%, as determined with trypan blue. The human tumour cytotoxicity was determined using the protein-binding dye sulforhodamine B (SRB) in a microculture assay to measure cell growth, as described in the protocols established by the NCI. A dose–response curve was plotted for each complex and the concentration (IC_{50}), resulting in an inhibition of 50% estimated through non-linear regression analysis. Results were expressed as inhibitory concentration 50 (IC_{50}) values.

4.5 Wound Healing Assay

To evaluate the effect of the curcumin derivatives in cell migration, a Wound healing assay was carried out, SK-LU-1 and U-251 cells were seeded in a 24-well plate at a density of 2.5 x 10^5 and 2 x 10^5 cells per well respectively, cultured 48 h at 38 °C and 5% CO_2, when confluence reached 90-100%, an artificial wound was generated on the cell monolayer using a 200 μL sterile micropipette tip and then washed with PBS to remove detached cells, PBS was removed and replaced with new supplemented medium or compounds dissolutions, different concentration were evaluated based on the IC_{50} values. For IC_{50} values between 0-4.9 μM a concentration of 5 μM was evaluated, between 5-9.9 μM a concentration of 10 μM was chosen and for values between 10-14.9 μM a concentration of 15 μM was tested, for curcumin concentration we considered the highest concentration of curcumin derivatives (15 μM in SK-LU-1 and 10 μM in U-251). The images were captured by an inverted microscope (DIAPHOT 300 Nikon®, Japan) with a digital camera (AmScope MD500) at 0 h, 24 h and

48h treatment. Wound areas were obtained using polygon selection and the Measure tool of ImageJ software. The relative migration ratio (%) was calculated by:

$$\text{Relative migration ratio (\%)} = \frac{(wound\ area\ t0 - wound\ area\ t24\ or\ t48)}{wound\ area\ t0} * 100$$

Results expressed triplicated experiments and significance was obtained by a 2way ANOVA with Tukey's multiple comparisons tests.

4.6 Computational details

Molecular docking

Performed docking simulations with them using potential protein targets for each cell line were one as follows: for chronic myelogenous leukemia (K-562) we used 14 targets among membrane receptors, tyrosine kinases, and cyclin-dependent kinases [34–37] (PDBs: 5VKM, 5XY1, 6HM6, 6HRP, 3CS9, 1FIN, 1W98, 2W96, 3G33, 3NUP, 1QPJ, 1XZ0, 2DQ7, and 4XJS);[38–48] for breast cancer (MCF-7) we used 5 targets among synthetases and progesterone and estrogen receptors [49–51] (PDBs: 2J6M, 3HY3, 4FA2, 4OAR, 6CHZ);[52–56] and 6 targets for lung cancer (SK-LU-1) among the epidermal growth factor and tyrosine kinases [57,58] (PDBs: 1M17, 3DKC, 3LMG, 3ZBF, 4CKJ, and 5FTO)[59–64]. These protein targets were prepared in the software Maestro 10.3 to a physiological pH of 7, removing water molecules and previous ligands.[65] Structures of compounds **L3** and **L3-Zn** were constructed on Gausview. Gasteiger charges were finally added in AutoDock Tools 1.5.6 for macromolecules and ligands. The docking simulations were carried out on AutoDock Vina 1.1.2 with an exhaustiveness parameter of 20,[66] and the results were analyzed. The binding site 3D representations were obtained with Maestro 10.3 whereas the 2D representations were made using LigPlot+.[67,68]

4.7 Determination of partition coefficients

Partition coefficients of Log *D* were measured according to the procedure 1b (hydrophobic compounds) method previously reported,[27] and the quantitation of the ligands and complexes was about 6.67 mg/mL was recorded by HPLC.

Procedure:

1. A buffer solution was prepared at pH 7.4 by dissolving 8.0 g of NaCl, 0.2 g of KCl, 1.44 g of Na_2HPO_4, and 0.24 g of KH_2PO_4 in 1000 mL of Milli-Q water. The pH was adjusted to 7.4 using HCl.

2. Saturating the mediums involves gently combining n-octanol with a pH 7.4 buffer solution and the buffer solution with n-octanol, allowing the two phases to equilibrate. This step is crucial to perform before conducting partition coefficient experiments.

3. Stock dissolution was prepared with 5 mg of ligand or complex in 750 µL of acetonitrile (6.67 mg / mL).

4. In a new vial was added 100 µL of stock solution and 1000 µL of buffer at pH 7.4 previously prepared, and a dilution 1:2 (r=2) was performed with acetonitrile to ensure that the compounds remained soluble <water standard solution>.

5. In a different vial, was added 100 µL of stock solution, 1000 µL of buffer pH 7.4 (Vw= 1000) and 20 µL of saturated *n*-octanol (Vo= 20). The mixture was stirred for 12 hours with a magnetic stir after the aqueous phase was separated and collocated in a new vial <water-partition solution>

Solutions: <water standard solution (Ast)> and < water-partition solution (Aw)> were chromatographed for analysis by HPLC.

6. The measurements were performed in an HPLC instrument with a UV-Vis Diode Array Waters 2996 Detector, Column: Kinetex 5 mm EVO C18 100 Å 100 x 2.1 mm. Vinj: 1 µL. The eluent was a mixture of acetonitrile/0.1% Formic acid (v/v) in water (4:6) in a Flow of 0.3 mL/min at room temperature. λ= 262 nm.

7. Calculate de Log (D) with the following formula:

$$Log\ (D) = \log\left(\frac{Ast}{Aw} * \frac{Vinj\ w}{Vinj\ st} * (r-1) * \frac{Vw}{Vo}\right)$$

Acknowledgements

A.A.-C. is grateful to CONAHCyT for a Postdoctoral Fellowship (estancias posdoctorales por México 2022(1)). A.S.-M. would like to thank CONAHCyT (No. CVU: 848539) and Fundación Telmex-Telcel (Folio: 212009996) for PhD scholarship. D.M.M. is grateful for the financial support of this research by PAPIIT-DGAPA-UNAM (PAPIIT IN223323) and CONACYT A1-S-033933. We are indebted to María de la Paz Orta Pérez (EA), Adriana

10.1002/cbdv.202402083

Romo (IR), Carmen Ríos (HPLC), Lucero Ríos Ruíz (ESI), Elizabeth Huerta Salazar (RMN); Martha Elena García Aguilera, Beatriz Quiroz García and Nuria Esturau Escofet (LURMN), from Instituto de Química UNAM.

Conflict of Interest

The authors declare no conflict of interest.

Data Availability Statement

The data that support the findings of this study are available in the supporting information of this article.

References

(1) Boarescu; Boarescu; Bocșan; Gheban; Bulboacă; Nicula; Pop; Râjnoveanu; Bolboacă. Antioxidant and Anti-Inflammatory Effects of Curcumin Nanoparticles on Drug-Induced Acute Myocardial Infarction in Diabetic Rats. *Antioxidants* **2019**, *8* (10), 504. https://doi.org/10.3390/antiox8100504.

(2) Jakubczyk, K.; Drużga, A.; Katarzyna, J.; Skonieczna-żydecka, K. Antioxidant Potential of Curcumin—a Meta-Analysis of Randomized Clinical Trials. *Antioxidants* **2020**, *9* (11), 1–13. https://doi.org/10.3390/antiox9111092.

(3) Ng, T. B. ; L. F. ; W. Z. T. Antioxidative Activity of Natural Products from Plants. *Life Sci* **2000**, *66*, 709–723.

(4) Al-Wabli, R. I.; AboulWafa, O. M.; Youssef, K. M. Synthesis of Curcumin and Ethylcurcumin Bioconjugates as Potential Antitumor Agents. *Medicinal Chemistry Research* **2012**, *21* (6), 874–890. https://doi.org/10.1007/s00044-011-9587-3.

(5) Zoi, V.; Galani, V.; Lianos, G. D.; Voulgaris, S.; Kyritsis, A. P.; Alexiou, G. A. The Role of Curcumin in Cancer Treatment. *Biomedicines* **2021**, *9* (9), 1086. https://doi.org/10.3390/biomedicines9091086.

(6) Devassy, J. G.; Nwachukwu, I. D.; Jones, P. J. H. Curcumin and Cancer: Barriers to Obtaining a Health Claim. *Nutr Rev* **2015**, *73* (3), 155–165. https://doi.org/10.1093/nutrit/nuu064.

(7) Dytrych, P.; Kejík, Z.; Hajduch, J.; Kaplánek, R.; Veselá, K.; Kučnirová, K.; Skaličková, M.; Venhauerová, A.; Hoskovec, D.; Martásek, P.; Jakubek, M. Therapeutic Potential and Limitations of Curcumin as Antimetastatic Agent. *Biomedicine and Pharmacotherapy*. Elsevier Masson s.r.l. July 1, 2023. https://doi.org/10.1016/j.biopha.2023.114758.

(8) Farghadani, R.; Naidu, R. Curcumin as an Enhancer of Therapeutic Efficiency of Chemotherapy Drugs in Breast Cancer. *International Journal of Molecular Sciences*. MDPI February 1, 2022. https://doi.org/10.3390/ijms23042144.

(9) Akbik, D.; Ghadiri, M.; Chrzanowski, W.; Rohanizadeh, R. Curcumin as a Wound Healing Agent. *Life Sci* **2014**, *116* (1), 1–7. https://doi.org/10.1016/j.lfs.2014.08.016.

(10) Mohanty, C.; Sahoo, S. K. Curcumin and Its Topical Formulations for Wound Healing Applications. *Drug Discov Today* **2017**, *22* (10), 1582–1592. https://doi.org/10.1016/j.drudis.2017.07.001.

(11) Anand, P.; Kunnumakkara, A. B.; Newman, R. A.; Aggarwal, B. B. Bioavailability of Curcumin: Problems and Promises. *Mol Pharm* **2007**, *4* (6), 807–818. https://doi.org/10.1021/mp700113r.

(12) Purpura, M.; Lowery, R. P.; Wilson, J. M.; Mannan, H.; Münch, G.; Razmovski-Naumovski, V. Analysis of Different Innovative Formulations of Curcumin for Improved Relative Oral Bioavailability in Human Subjects. *Eur J Nutr* **2018**, *57* (3), 929–938. https://doi.org/10.1007/s00394-016-1376-9.

(13) Prasad, S.; Tyagi, A. K.; Aggarwal, B. B. Recent Developments in Delivery, Bioavailability, Absorption and Metabolism of Curcumin: The Golden Pigment from Golden Spice. *Cancer Res Treat* **2014**, *46* (1), 2–18. https://doi.org/10.4143/crt.2014.46.1.2.

(14) Lei, F.; Li, P.; Chen, T.; Wang, Q.; Wang, C.; Liu, Y.; Deng, Y.; Zhang, Z.; Xu, M.; Tian, J.; Ren, W.; Li, C. Recent Advances in Curcumin-Loaded Biomimetic Nanomedicines for Targeted Therapies. *J Drug Deliv Sci Technol* **2023**, *80*, 104200. https://doi.org/10.1016/j.jddst.2023.104200.

(15) Sohn, S.-I.; Priya, A.; Balasubramaniam, B.; Muthuramalingam, P.; Sivasankar, C.; Selvaraj, A.; Valliammai, A.; Jothi, R.; Pandian, S. Biomedical Applications and Bioavailability of Curcumin—An Updated Overview. *Pharmaceutics* **2021**, *13* (12), 2102. https://doi.org/10.3390/pharmaceutics13122102.

(16) Gunathilake, T. M. S. U.; Ching, Y. C.; Chuah, C. H. Enhancement of Curcumin Bioavailability Using Nanocellulose Reinforced Chitosan Hydrogel. *Polymers (Basel)* **2017**, *9* (2), 64. https://doi.org/10.3390/polym9020064.

(17) Sareen, R.; Jain, N.; Dhar, K. L. Curcumin–Zn(II) Complex for Enhanced Solubility and Stability: An Approach for Improved Delivery and Pharmacodynamic Effects. *Pharm Dev Technol* **2016**, *21* (5), 630–635. https://doi.org/10.3109/10837450.2015.1041042.

(18) Su, H.; Sun, F.; Jia, J.; He, H.; Wang, A.; Zhu, G. A Highly Porous Medical Metal–Organic Framework Constructed from Bioactive Curcumin. *Chemical Communications* **2015**, *51* (26), 5774–5777. https://doi.org/10.1039/C4CC10159F.

(19) Al-Noor, T. H.; Ali, A. M.; Al-Sarray, A. J. A.; Al-Obaidi, O. H.; Obeidat, A. I. M.; Habash, R. R. A Short Review: Chemistry of Curcumin and Its Metal Complex Derivatives. **2022**.

(20) Prasad, S.; Dubourdieu, D.; Srivastava, A.; Kumar, P.; Lall, R. Metal–Curcumin Complexes in Therapeutics: An Approach to Enhance Pharmacological Effects of Curcumin. *International Journal of Molecular Sciences*. MDPI July 1, 2021. https://doi.org/10.3390/ijms22137094.

(21) Xue, X.; Wang, J.; Si, G.; Wang, C.; Zhou, S. Synthesis, DNA-Binding Properties and Cytotoxicity Evaluation of Two Copper(II) Complexes Based on Curcumin. *Transition Metal Chemistry* **2016**, *41* (3), 331–337. https://doi.org/10.1007/s11243-016-0027-6.

(22) Xu, G.; Wang, J.; Liu, T.; Wang, M.; Zhou, S.; Wu, B.; Jiang, M. Synthesis and Crystal Structure of a Novel Copper(II) Complex of Curcumin-Type and Its Application in in Vitro and in Vivo Imaging. *J Mater Chem B* **2014**, *2* (23), 3659–3666. https://doi.org/10.1039/c4tb00133h.

(23) Obstarczyk, P.; Pniakowska, A.; Nonappa; Grzelczak, M. P.; Olesiak-Bańska, J. Crown Ether-Capped Gold Nanoclusters as a Multimodal Platform for Bioimaging. *ACS Omega* **2023**, *8* (12), 11503–11511. https://doi.org/10.1021/acsomega.3c00426.

(24) Kralj, M.; Tušek-Božić, L.; Frkanec, L. Biomedical Potentials of Crown Ethers: Prospective Antitumor Agents. *ChemMedChem* **2008**, *3* (10), 1478–1492. https://doi.org/10.1002/cmdc.200800118.

(25) Baraldi, P. G.; Preti, D.; Tabrizi, M. A.; Fruttarolo, F.; Saponaro, G.; Baraldi, S.; Romagnoli, R.; Moorman, A. R.; Gessi, S.; Varani, K.; Borea, P. A. N6-[(Hetero)Aryl/(Cyclo)Alkyl-Carbamoyl-Methoxy-Phenyl]-(2-Chloro)-5′-N-Ethylcarboxamido-Adenosines: The First Example of Adenosine-Related Structures with Potent Agonist Activity at the Human A2B

Adenosine Receptor. *Bioorg Med Chem* **2007**, *15* (7), 2514–2527. https://doi.org/10.1016/j.bmc.2007.01.055.

(26) Schmitt, F.; Gold, M.; Begemann, G.; Andronache, I.; Biersack, B.; Schobert, R. Fluoro and Pentafluorothio Analogs of the Antitumoral Curcuminoid EF24 with Superior Antiangiogenic and Vascular-Disruptive Effects. *Bioorg Med Chem* **2017**, *25* (17), 4894–4903. https://doi.org/10.1016/j.bmc.2017.07.039.

(27) Andrés, A.; Rosés, M.; Ràfols, C.; Bosch, E.; Espinosa, S.; Segarra, V.; Huerta, J. M. Setup and Validation of Shake-Flask Procedures for the Determination of Partition Coefficients (LogD) from Low Drug Amounts. *European Journal of Pharmaceutical Sciences* **2015**, *76*, 181–191. https://doi.org/10.1016/j.ejps.2015.05.008.

(28) Priyadarsini, K. I. Photophysics, Photochemistry and Photobiology of Curcumin: Studies from Organic Solutions, Bio-Mimetics and Living Cells. *Journal of Photochemistry and Photobiology C: Photochemistry Reviews* **2009**, *10* (2), 81–95. https://doi.org/10.1016/j.jphotochemrev.2009.05.001.

(29) Zsila, F.; Bikádi, Z.; Simonyi, M. Unique, PH-Dependent Biphasic Band Shape of the Visible Circular Dichroism of Curcumin–Serum Albumin Complex. *Biochem Biophys Res Commun* **2003**, *301* (3), 776–782. https://doi.org/10.1016/S0006-291X(03)00030-5.

(30) Jagannathan, R.; Abraham, P. M.; Poddar, P. Temperature-Dependent Spectroscopic Evidences of Curcumin in Aqueous Medium: A Mechanistic Study of Its Solubility and Stability. *J Phys Chem B* **2012**, *116* (50), 14533–14540. https://doi.org/10.1021/jp3050516.

(31) Patra, D.; Barakat, C. Synchronous Fluorescence Spectroscopic Study of Solvatochromic Curcumin Dye. *Spectrochim Acta A Mol Biomol Spectrosc* **2011**, *79* (5), 1034–1041. https://doi.org/10.1016/j.saa.2011.04.016.

(32) Obregón-Mendoza, M. A.; Meza-Morales, W.; Alvarez-Ricardo, Y.; Estévez-Carmona, M. M.; Enríquez, R. G. High Yield Synthesis of Curcumin and Symmetric Curcuminoids: A "Click" and "Unclick" Chemistry Approach. *Molecules* **2022**, *28* (1), 289. https://doi.org/10.3390/molecules28010289.

(33) Origin Lab Corporation. *Origin(Pro), Version 8.5.1*; Northampton, MA, USA.

(34) D'cruz, O. J.; Uckun, F. M. Protein Kinase Inhibitors against Malignant Lymphoma. *Expert Opinion on Pharmacotherapy*. 2013, pp 707–721. https://doi.org/10.1517/14656566.2013.780031.

(35) Salvaris, R.; Fedele, P. L. Targeted Therapy in Acute Lymphoblastic Leukaemia. *Journal of Personalized Medicine*. 2021. https://doi.org/10.3390/jpm11080715.

(36) Brown, V. I.; Seif, A. E.; Reid, G. S. D.; Teachey, D. T.; Grupp, S. A. Novel Molecular and Cellular Therapeutic Targets in Acute Lymphoblastic Leukemia and Lymphoproliferative Disease. *Immunologic Research*. 2008, pp 84–105. https://doi.org/10.1007/s12026-008-8038-9.

(37) Jayaraman, A.; Jamil, K. Drug Targets for Cell Cycle Dysregulators in Leukemogenesis: In Silico Docking Studies. *PLoS One* **2014**, *9* (1). https://doi.org/10.1371/journal.pone.0086310.

(38) Weisberg, E.; Manley, P. W.; Breitenstein, W.; Brüggen, J.; Cowan-Jacob, S. W.; Ray, A.; Huntly, B.; Fabbro, D.; Fendrich, G.; Hall-Meyers, E.; Kung, A. L.; Mestan, J.; Daley, G. Q.; Callahan, L.; Catley, L.; Cavazza, C.; Mohammed, A.; Neuberg, D.; Wright, R. D.; Gilliland, D. G.; Griffin, J. D. Characterization of AMN107, a Selective Inhibitor of Native and Mutant Bcr-Abl. *Cancer Cell* **2005**, *7* (2), 129–141. https://doi.org/10.1016/j.ccr.2005.01.007.

(39) Ereño-Orbea, J.; Sicard, T.; Cui, H.; Mazhab-Jafari, M. T.; Benlekbir, S.; Guarné, A.; Rubinstein, J. L.; Julien, J. P. Molecular Basis of Human CD22 Function and Therapeutic Targeting. *Nat Commun* **2017**, *8* (1), 1–11. https://doi.org/10.1038/s41467-017-00836-6.

(40) Barker, M. D.; Liddle, J.; Atkinson, F. L.; Wilson, D. M.; Dickson, M. C.; Ramirez-Molina, C.; Lewis, H.; Davis, R. P.; Somers, D. O.; Neu, M.; Jones, E.; Watson, R. Discovery of Potent and Selective Spleen Tyrosine Kinase Inhibitors for the Topical Treatment of Inflammatory Skin Disease. *Bioorg Med Chem Lett* **2018**, *28* (21), 3458–3462. https://doi.org/10.1016/j.bmcl.2018.09.022.

(41) Lopez-Tapia, F.; Lou, Y.; Brotherton-Pleiss, C.; Kuglstatter, A.; So, S.; Kondru, R. A Potent Seven-Membered Cyclic BTK (Bruton's Tyrosine Kinase) Chiral Inhibitor Conceived by Structure-Based Drug Design to Lock Its Bioactive Conformation. *Bioorg Med Chem Lett* **2019**, *29* (9), 1074–1078. https://doi.org/10.1016/j.bmcl.2019.03.001.

(42) Zhu, X.; Kim, J. L.; Newcomb, J. R.; Rose, P. E.; Stover, D. R.; Toledo, L. M.; Zhao, H.; Morgenstern, K. A. Structural Analysis of the Lymphocyte-Specific Kinase Lck in Complex with Non-Selective and Src Family Selective Kinase Inhibitors. *Structure* **1999**, *7* (6), 651–661. https://doi.org/10.1016/S0969-2126(99)80086-0.

(43) Zajonc, D. M.; Crispin, M. D. M.; Bowden, T. A.; Young, D. C.; Cheng, T. Y.; Hu, J.; Costello, C. E.; Rudd, P. M.; Dwek, R. A.; Miller, M. J.; Brenner, M. B.; Moody, D. B.; Wilson, I. A. Molecular Mechanism of Lipopeptide Presentation by CD1a. *Immunity* **2005**, *22* (2), 209–219. https://doi.org/10.1016/j.immuni.2004.12.009.

(44) Kinoshita, T.; Matsubara, M.; Ishiguro, H.; Okita, K.; Tada, T. Structure of Human Fyn Kinase Domain Complexed with Staurosporine. *Biochem Biophys Res Commun* **2006**, *346* (3), 840–844. https://doi.org/10.1016/j.bbrc.2006.05.212.

(45) Becherer, J. D.; Boros, E. E.; Carpenter, T. Y.; Cowan, D. J.; Deaton, D. N.; Haffner, C. D.; Jeune, M. R.; Kaldor, I. W.; Poole, J. C.; Preugschat, F.; Rheault, T. R.; Schulte, C. A.; Shearer, B. G.; Shearer, T. W.; Shewchuk, L. M.; Smalley, T. L.; Stewart, E. L.; Stuart, J. D.; Ulrich, J. C. Discovery of 4-Amino-8-Quinoline Carboxamides as Novel, Submicromolar Inhibitors of NAD-Hydrolyzing Enzyme CD38. *J Med Chem* **2015**, *58* (17), 7021–7056. https://doi.org/10.1021/acs.jmedchem.5b00992.

(46) Honda, R.; Lowe, E. D.; Dubinina, E.; Skamnaki, V.; Cook, A.; Brown, N. R.; Johnson, L. N. The Structure of Cyclin E1/CDK2: Implications for CDK2 Activation and CDK2-Independent Roles. *EMBO Journal* **2005**, *24* (3), 452–463. https://doi.org/10.1038/sj.emboj.7600554.

(47) Day, P. J.; Cleasby, A.; Tickle, I. J.; O'Reilly, M.; Coyle, J. E.; Holding, F. P.; McMenamin, R. L.; Yon, J.; Chopra, R.; Lengauer, C.; Jhoti, H. Crystal Structure of Human CDK4 in Complex with a D-Type Cyclin. *Proc Natl Acad Sci U S A* **2009**, *106* (11), 4166–4170. https://doi.org/10.1073/pnas.0809645106.

(48) Takaki, T.; Echalier, A.; Brown, N. R.; Hunt, T.; Endicott, J. A.; Noble, M. E. M. The Structure of CDK4/Cyclin D3 Has Implications for Models of CDK Activation. *Proc Natl Acad Sci U S A* **2009**, *106* (11), 4171–4176. https://doi.org/10.1073/pnas.0809674106.

(49) Amin, K. M.; Syam, Y. M.; Anwar, M. M.; Ali, H. I.; Abdel-Ghani, T. M.; Serry, A. M. Synthesis and Molecular Docking Studies of New Furochromone Derivatives as P38α MAPK Inhibitors Targeting Human Breast Cancer MCF-7 Cells. *Bioorg Med Chem* **2017**, *25* (8), 2423–2436. https://doi.org/10.1016/j.bmc.2017.02.065.

(50) Mass, E. B.; de Lima, C. A.; D'Oca, M. G. M.; Sciani, J. M.; Longato, G. B.; Russowsky, D. Synthesis, Selective Cytotoxic Activity against Human Breast Cancer MCF7 Cell Line and Molecular Docking of Some Chalcone-Dihydropyrimidone Hybrids. *Drugs and Drug Candidates* **2022**, *1* (1), 3–21. https://doi.org/10.3390/ddc1010002.

(51) Acharya, R.; Chacko, S.; Bose, P.; Lapenna, A.; Pattanayak, S. P. Structure Based Multitargeted Molecular Docking Analysis of Selected Furanocoumarins against Breast Cancer. *Sci Rep* **2019**, *9* (1), 15743. https://doi.org/10.1038/s41598-019-52162-0.

(52) Yun, C.-H.; Boggon, T. J.; Li, Y.; Woo, M. S.; Greulich, H.; Meyerson, M.; Eck, M. J. Structures of Lung Cancer-Derived EGFR Mutants and Inhibitor Complexes: Mechanism of Activation and Insights into Differential Inhibitor Sensitivity. *Cancer Cell* **2007**, *11* (3), 217–227. https://doi.org/10.1016/j.ccr.2006.12.017.

(53) Wu, D.; Li, Y.; Song, G.; Cheng, C.; Zhang, R.; Joachimiak, A.; Shaw, N.; Liu, Z.-J. Structural Basis for the Inhibition of Human 5,10-Methenyltetrahydrofolate Synthetase by N10-Substituted Folate Analogues. *Cancer Res* **2009**, *69* (18), 7294–7301. https://doi.org/10.1158/0008-5472.CAN-09-1927.

(54) Watterson, D. M.; Grum-Tokars, V. L.; Roy, S. M.; Schavocky, J. P.; Bradaric, B. D.; Bachstetter, A. D.; Xing, B.; Dimayuga, E.; Saeed, F.; Zhang, H.; Staniszewski, A.; Pelletier, J. C.; Minasov, G.; Anderson, W. F.; Arancio, O.; Van Eldik, L. J. Development of Novel In Vivo Chemical Probes to Address CNS Protein Kinase Involvement in Synaptic Dysfunction. *PLoS One* **2013**, *8* (6), e66226. https://doi.org/10.1371/journal.pone.0066226.

(55) Petit-Topin, I.; Fay, M.; Resche-Rigon, M.; Ulmann, A.; Gainer, E.; Rafestin-Oblin, M.-E.; Fagart, J. Molecular Determinants of the Recognition of Ulipristal Acetate by Oxo-Steroid Receptors. *J Steroid Biochem Mol Biol* **2014**, *144*, 427–435. https://doi.org/10.1016/j.jsbmb.2014.08.008.

(56) Puyang, X.; Furman, C.; Zheng, G. Z.; Wu, Z. J.; Banka, D.; Aithal, K.; Agoulnik, S.; Bolduc, D. M.; Buonamici, S.; Caleb, B.; Das, S.; Eckley, S.; Fekkes, P.; Hao, M.-H.; Hart, A.; Houtman, R.; Irwin, S.; Joshi, J. J.; Karr, C.; Kim, A.; Kumar, N.; Kumar, P.; Kuznetsov, G.; Lai, W. G.; Larsen, N.; Mackenzie, C.; Martin, L.-A.; Melchers, D.; Moriarty, A.; Nguyen, T.-V.; Norris, J.; O'Shea, M.; Pancholi, S.; Prajapati, S.; Rajagopalan, S.; Reynolds, D. J.; Rimkunas, V.; Rioux, N.; Ribas, R.; Siu, A.; Sivakumar, S.; Subramanian, V.; Thomas, M.; Vaillancourt, F. H.; Wang, J.; Wardell, S.; Wick, M. J.; Yao, S.; Yu, L.; Warmuth, M.; Smith, P. G.; Zhu, P.; Korpal, M. Discovery of Selective Estrogen Receptor Covalent Antagonists for the Treatment of ERαWT and ERαMUT Breast Cancer. *Cancer Discov* **2018**, *8* (9), 1176–1193. https://doi.org/10.1158/2159-8290.CD-17-1229.

(57) Hidayat, S.; Ibrahim, F. M.; Suhandi, C.; Muchtaridi, M. A Systematic Review: Molecular Docking Simulation of Small Molecules as Anticancer Non-Small Cell Lung Carcinoma Drug Candidates. *J Adv Pharm Technol Res* **2022**, *13* (3), 141–147. https://doi.org/10.4103/japtr.japtr_311_21.

(58) Shtivelman, E.; Hensing, T.; Simon, G. R.; Dennis, P. A.; Otterson, G. A.; Bueno, R.; Salgia, R. Molecular Pathways and Therapeutic Targets in Lung Cancer. *Oncotarget* **2014**, *5* (6), 1392–1433. https://doi.org/10.18632/oncotarget.1891.

(59) Stamos, J.; Sliwkowski, M. X.; Eigenbrot, C. Structure of the Epidermal Growth Factor Receptor Kinase Domain Alone and in Complex with a 4-Anilinoquinazoline Inhibitor. *Journal of Biological Chemistry* **2002**, *277* (48), 46265–46272. https://doi.org/10.1074/jbc.M207135200.

(60) Buchanan, S. G.; Hendle, J.; Lee, P. S.; Smith, C. R.; Bounaud, P.-Y.; Jessen, K. A.; Tang, C. M.; Huser, N. H.; Felce, J. D.; Froning, K. J.; Peterman, M. C.; Aubol, B. E.; Gessert, S. F.; Sauder, J. M.; Schwinn, K. D.; Russell, M.; Rooney, I. A.; Adams, J.; Leon, B. C.; Do, T. H.; Blaney, J. M.; Sprengeler, P. A.; Thompson, D. A.; Smyth, L.; Pelletier, L. A.; Atwell, S.; Holme, K.; Wasserman, S. R.; Emtage, S.; Burley, S. K.; Reich, S. H. SGX523 Is an Exquisitely Selective, ATP-Competitive Inhibitor of the MET Receptor Tyrosine Kinase with Antitumor Activity in Vivo. *Mol Cancer Ther* **2009**, *8* (12), 3181–3190. https://doi.org/10.1158/1535-7163.MCT-09-0477.

(61) Shi, F.; Telesco, S. E.; Liu, Y.; Radhakrishnan, R.; Lemmon, M. A. ErbB3/HER3 Intracellular Domain Is Competent to Bind ATP and Catalyze Autophosphorylation. *Proceedings of the National Academy of Sciences* **2010**, *107* (17), 7692–7697. https://doi.org/10.1073/pnas.1002753107.

(62) Awad, M. M.; Katayama, R.; McTigue, M.; Liu, W.; Deng, Y.-L.; Brooun, A.; Friboulet, L.; Huang, D.; Falk, M. D.; Timofeevski, S.; Wilner, K. D.; Lockerman, E. L.; Khan, T. M.; Mahmood, S.; Gainor, J. F.; Digumarthy, S. R.; Stone, J. R.; Mino-Kenudson, M.; Christensen, J. G.; Iafrate, A. J.; Engelman, J. A.; Shaw, A. T. Acquired Resistance to Crizotinib from a Mutation in CD74 – ROS1. *New England Journal of Medicine* **2013**, *368* (25), 2395–2401. https://doi.org/10.1056/NEJMoa1215530.

(63) Plaza-Menacho, I.; Barnouin, K.; Goodman, K.; Martínez-Torres, R. J.; Borg, A.; Murray-Rust, J.; Mouilleron, S.; Knowles, P.; McDonald, N. Q. Oncogenic RET Kinase Domain Mutations Perturb the Autophosphorylation Trajectory by Enhancing Substrate Presentation In Trans. *Mol Cell* **2014**, *53* (5), 738–751. https://doi.org/10.1016/j.molcel.2014.01.015.

(64) Menichincheri, M.; Ardini, E.; Magnaghi, P.; Avanzi, N.; Banfi, P.; Bossi, R.; Buffa, L.; Canevari, G.; Ceriani, L.; Colombo, M.; Corti, L.; Donati, D.; Fasolini, M.; Felder, E.; Fiorelli, C.; Fiorentini, F.; Galvani, A.; Isacchi, A.; Borgia, A. L.; Marchionni, C.; Nesi, M.; Orrenius, C.; Panzeri, A.; Pesenti, E.; Rusconi, L.; Saccardo, M. B.; Vanotti, E.; Perrone, E.; Orsini, P. Discovery of Entrectinib: A New 3-Aminoindazole As a Potent Anaplastic Lymphoma Kinase (ALK), c-Ros Oncogene 1 Kinase (ROS1), and Pan-Tropomyosin Receptor Kinases (Pan-TRKs) Inhibitor. *J Med Chem* **2016**, *59* (7), 3392–3408. https://doi.org/10.1021/acs.jmedchem.6b00064.

(65) *Schrödinger Release 2023-3: Maestro, Schrödinger*; LLC, New York, NY, 2023.

(66) Trott, O.; Olson, A. J. AutoDock Vina: Improving the Speed and Accuracy of Docking with a New Scoring Function, Efficient Optimization, and Multithreading. *J Comput Chem* **2009**, NA-NA. https://doi.org/10.1002/jcc.21334.

(67) Laskowski, R. A.; Swindells, M. B. LigPlot+: Multiple Ligand–Protein Interaction Diagrams for Drug Discovery. *J Chem Inf Model* **2011**, *51* (10), 2778–2786. https://doi.org/10.1021/ci200227u.

(68) Wallace, A. C.; Laskowski, R. A.; Thornton, J. M. LIGPLOT: A Program to Generate Schematic Diagrams of Protein-Ligand Interactions. *"Protein Engineering, Design and Selection"* **1995**, *8* (2), 127–134. https://doi.org/10.1093/protein/8.2.127.